# A Quantitative Analysis of the Separation of Aluminum Cans Out of a Waste Stream Based on Eddy Current Induced Levitation

Martin Woltereck, *Student Member, IEEE*, Reinhold Ludwig, *Senior Member, IEEE*, and William Michalson

*Abstract*—**Eddy current induced levitation can be employed to separate conducting from nonconducting materials as in the recycling of aluminum products. To investigate magnetic fields, eddy currents, and forces, a multiple strategy involving analytical, numerical, and experimental analysis techniques is implemented.**

**In particular, the configuration of an aluminum can over an arrangement of multiple coils is investigated with a two-dimensional parametric finite element model. The results from these simulations are compared to measurements of a practical levitation device.**

**To establish the fidelity of the finite element model, we applied the method to two simplified geometries of a thick and a thin slab extended over a conducting wire. For the first case, an analytical inverse Laplace-transform model for the eddy current density is developed. For the second case, Lorentz forces exerted on the thin slab are analytically obtained by employing Maxwell's moving image method. In addition, an approximation to the moving image method is derived which can be described by an equivalent resonance circuit.**

## I. Introduction

### A. Background

ALTHOUGH municipal waste contains only approximately 1% nonferrous material, it nonetheless accounts for a large potential revenue that could be achieved through the resale of separated products. In particular, recycling of aluminum helps to reduce landfills and saves valuable raw materials. In order to recycle aluminum, it has to be separated out of a commingled waste stream, a process commonly carried out in source separation facilities where ferromagnetic materials are first removed via head pulley magnets or drum magnets [1].

Methods for the separation of aluminum from the remaining waste stream include manual separation as well as density separation methods such as hydraulic or pneumatic classifiers [2]. These methods are either labor intensive or of limited applicability since many plastics have the same density as aluminum. For fine-shredded material, both electrostatic methods [3] and magnetofluid separators [4] are employed.

Manuscript received October 3, 1995; revised May 3, 1996.

The authors are with the Electrical and Computer Engineering Department, Worcester Polytechnic Institute, Worcester, MA 01609-2280.

Publisher Item Identifier S 0018-9464(97)00116-7.

More recently, very promising methods have been developed based on the idea of eddy current separation [1], [5]. An alternating magnetic field induces eddy currents in conducting bodies which in turn combine with the magnetic field to cause a Lorentz force which is capable of accelerating conducting materials away from nonconducting products. For recycling systems, the alternating magnetic field is achieved by a relative motion of the conducting bodies with respect to one or more permanent magnets. This method has been quantitatively investigated for a ramp separator [7], [8] as well as a single boundary separator [9]–[11].

Because of their ruggedness, rotating magnet separators are often employed for industrial applications. Here the waste stream is transported on a conveyor belt which is redirected by a drum. Within the conveyor belt roller, a set of permanent magnets rotates in the opposite direction of the belt. Lorentz forces act on the conducting materials decelerating and lifting them in a different trajectory from those of nonconducting materials (as shown in Fig. 1).

The objective of this paper is to present a new approach whereby the alternating magnetic field is created with ac-fed coils. This concept avoids the mechanical limitations of a rotating drum. The coils are compact, not subject to wear and tear, and readily operational over a wide range of excitation frequencies.

### B. Approach

For the ac-fed coil, a numerical modeling formulation based on the finite element method is developed in order to calculate the magnetic fields, induced eddy currents, and resulting Lorentz forces. The finite element model is tested against two analytical solutions. First, it is shown that the results for the eddy current distribution, derived by an inverse Laplace-transform model of an infinite wire suspended under a conducting half-space, is in excellent agreement with the predictions made by the finite element model.

Second, the model of a thin conducting slab over an infinite wire is investigated. A formula for the resulting Lorentz forces exerted on the slab is derived by employing the moving image method. This method was first introduced by Maxwell, but it is rarely used in practical

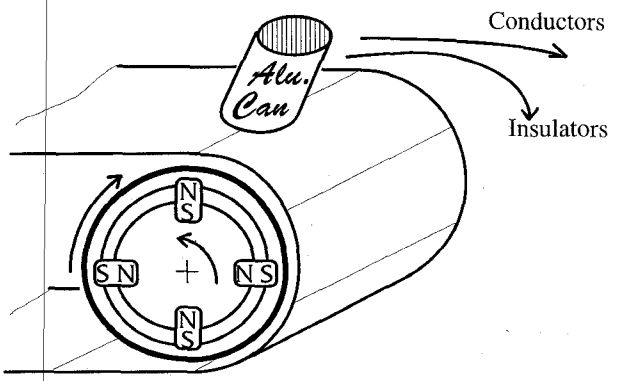


Fig. 1. Waste separation with rotating magnets.

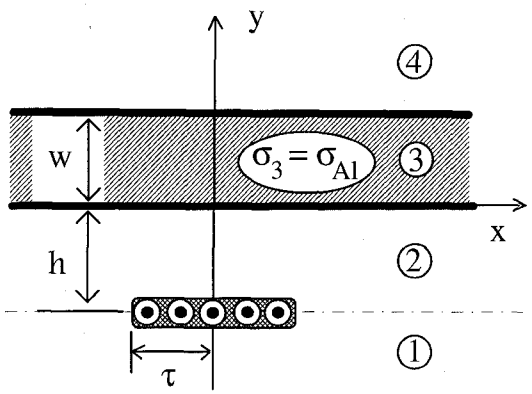


Fig. 2. Geometric arrangement of conducting slab over a strip conductor.

applications. In addition, an analog with an equivalent electrical circuit provides an easy to handle approximation for the force prediction. Although the testing of numerical models by various analytical solutions has been reported before, the moving image method is a novel approach to verify finite element force predictions for thin nonferrous plates.

Finally, our numerical model is applied to the geometry of a realistic application: the field behavior of an aluminum can above an arrangement of multiple coils. The results of these computer simulations are tested against practical measurements, in order to obtain suggestions for the excitation arrangement, optimal frequency, and a possible levitation configuration.

## II. Formulation

In order to find an analytical formulation for the induced eddy current density $\boldsymbol{J}_e$, it is helpful to reduce the problem to a simplified two-dimensional model in the $x$-$y$ plane. A simple geometry consists of four layers ($\nu = 1, \cdots, 4$) as shown in Fig. 2. An aluminum plate or slab of the conductivity $\sigma_3 = \sigma_{Al}$ is located over a long, straight conductor of width $\tau$ which is extended infinitely in the $z$-direction and carries the source current $J_{s,z}$. All currents and fields are sinusoidal functions of the angular excitation frequency $\omega$. Since the material is nonferrous, the magnetic permeability equals $\mu_0$ everywhere.

The basis for the numerical and analytical treatments of induced eddy currents is the inhomogeneous, parabolic partial differential equation involving the single component of the magnetic vector potential $A_z$ in the form

$$\frac{\partial^2 A_z}{\partial x^2} + \frac{\partial^2 A_z}{\partial y^2} - \mu_0 \sigma_\nu \frac{\partial A_z}{\partial t} = -\mu_0 J_{s,z} \quad \text{with} \begin{cases} \sigma_\nu = \sigma_{Al} & \text{for } \nu = 3 \\ \sigma_\nu = 0 & \text{for } \nu \neq 3. \end{cases} \tag{1}$$

The induced eddy current density is identified by the term

$$J_{e,z} = -\sigma_3 \frac{\partial A}{\partial t} = -j\omega\sigma_3 A. \tag{2}$$

Since only the $z$-components of the vectors $\boldsymbol{A}$, $\boldsymbol{J}_s$, and $\boldsymbol{J}_e$, are involved, the subscript $z$ is subsequently omitted.

The boundary conditions in terms of the normal and tangential components of the magnetic flux density and the magnetic field can be expressed as vector potentials and can be applied to the four layers as follows:

$$A_{\nu+1} = A_\nu \tag{3}$$

$$\frac{\partial A_{\nu+1}}{\partial y} - \frac{\partial A_\nu}{\partial y} = \begin{cases} \hat{I}_s \mu_0 & \text{for } \nu = 1 \\ 0 & \text{for } \nu \neq 1. \end{cases} \tag{4}$$

Here the current distribution in the strip conductor $\hat{I}_s$ can be written as the sum of two unit step functions

$$\hat{I}_s = \frac{I_s[u(x+\tau) - u(x-\tau)]}{2\tau}$$

where $I_s$ denotes the total source current in the strip conductor, and $u(x)$ is the Heaviside step function.

### A. Finite Element Approach

The finite element approach is employed to solve the underlying equation (1) for arbitrary two-dimensional geometries. This is carried out by employing the well-documented weighted residual method [11], which relies on the local approximation of the unknown potential and known current density by basis functions $\phi_i$ ($i$ denotes the nodes in the solution domain $\Omega$) such that

$$A = \sum_{j=1}^{k} A_j \phi_j \quad \text{and} \quad J_s = \sum_{j=1}^{k} J_{s,j} \phi_j. \tag{5}$$

Forming the inner product in the Galerkin sense and integration by parts yields [12]

$$\sum_{j=1}^{k} \int_L \phi_i \left.\frac{\partial A}{\partial n}\right|_j ndl = \sum_{j=1}^{k} \left[ \left\langle \frac{\partial \phi_i}{\partial x}\frac{\partial \phi_j}{\partial x} + \frac{\partial \phi_i}{\partial y}\frac{\partial \phi_j}{\partial y} \right\rangle A_j + \langle \mu_0 \sigma_j \phi_i \phi_j \rangle \frac{\partial A_j}{\partial t} - \langle \mu_0 \phi_i \phi_j \rangle J_{s,j} \right] \tag{6}$$

where the brackets $\langle\ \rangle$ denote the inner product in Hilbert space. The integration of the vector potential over the boundary ($n$ is the outward pointing normal) on the left-hand side constitutes the Neumann-type boundary condition. Rewriting (6) in conventional matrix notation yields

$$\{Q\} = [S]\{A\} + j\omega[C]\{A\} - [D]\{J\} \quad (7)$$

where the nodal point values for the magnetic vector potential and the current densities are given by the vectors $\{A\}$ and $\{J\}$. The matrices $[S]$, $[C]$, and $[D]$ contain the local domain integrals, and $\{Q\}$ represents the surface integral vector as specified in (6).

The above elemental matrices and vectors are assembled into a banded global triangularized matrix which can subsequently be solved for the global field $\{A\}$. From the magnetic vector potential, all quantities of interest can be derived. The total flux density $\boldsymbol{B}$ is calculated according to $\nabla \times \boldsymbol{A} = \boldsymbol{B}$. To obtain the induced eddy current density, the complex time derivative of $\boldsymbol{A}$ is formed

$$\mathrm{Re}(\boldsymbol{J}_e) = \mathrm{Im}(\boldsymbol{A})\,\omega\sigma \quad \text{and} \quad \mathrm{Im}(\boldsymbol{J}_e) = -\mathrm{Re}(\boldsymbol{A})\,\omega\sigma. \quad (8)$$

The Lorentz force density $\boldsymbol{f} = \boldsymbol{J}_e \times \boldsymbol{B}$ can be divided into a time averaged portion $\boldsymbol{f}_a$ and a part oscillating at twice the frequency. Since the mechanical time constants are assumed to be much larger than the oscillation time, only $\boldsymbol{f}_a$ is of interest for the subsequent applications. The two components of the force density are

$$f_{a,x} = \mathrm{Re}(J_e)\cdot\mathrm{Re}(B_y) + \mathrm{Im}(J_e)\cdot\mathrm{Im}(B_y) \quad (9a)$$

$$f_{a,y} = \mathrm{Re}(J_e)\cdot\mathrm{Re}(B_x) + \mathrm{Im}(J_e)\cdot\mathrm{Im}(B_x). \quad (9b)$$

This force density is integrated over the boundary assuming a unit thickness in $z$-direction to calculate the total force $\boldsymbol{F}$.

## III. Analytical Model Verification

### A. Thick Plate

In order to test the finite element model against a relatively simple analytical formulation, it is assumed that the thickness $w$ of the plate in the above model (Fig. 2) becomes large with respect to the skin depth $\phi = \sqrt{2/\omega\mu_0\sigma}$ whereby layer 4 can be neglected.

To eliminate $x$ and to obtain a function which depends on one variable only, the Fourier transformation

$$A(k, y) = \int_{-\infty}^{\infty} A(x, y)e^{-jkx}\,dx \quad (10)$$

is employed [13]. When applied to (1), it yields for the layers $\nu = 1 \cdots 3$

$$k^2A(k, y) - \frac{\partial^2 A(k, y)}{\partial y^2} = j\omega A\mu_0\sigma_\nu \quad (11)$$

and for the interface condition (4)

$$\frac{\partial A_2(y = -h, k)}{\partial y} - \frac{\partial A_1(y = -h, k)}{\partial y} = \hat{I}\tau\mu_0\,\mathrm{sinc}\,(\tau k) \quad (12a)$$

$$\frac{\partial A_3(y = 0, k)}{\partial y} - \frac{\partial A_2(y = 0, k)}{\partial y} = 0 \quad (12b)$$

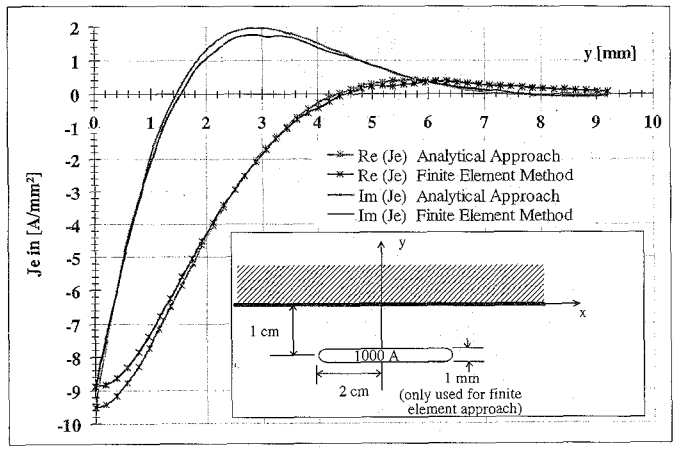


Fig. 3. Eddy current distribution inside an infinitely thick slab at a frequency of $f = 2$ kHz calculated by the analytical formulation (15) and by using the finite element method.

where $\mathrm{sinc}(\tau k)$ is the short-hand notation for $\sin(\tau k)/\tau k$. A general solution for (11) can be constructed for the 3 layers

$$A_1(k, y) = C_1 \cdot e^{-k(-y-h)} \quad (13a)$$

$$A_2(k, y) = C_2 \cdot e^{-k(-y+h)} + D_2e^{+k(-y-h)} \quad (13b)$$

$$A_3(k, y) = C_3 \cdot e^{-\gamma y} \quad (13c)$$

where $\gamma = \sqrt{k^2 + j\omega\sigma\mu_0}$. Note that (13a) and (13c) do not involve any increasing exponential terms since $A_1$ and $A_3$ should converge to zero at infinity.

By inserting (13a)–(13c) into the boundary conditions (3), (12a), and (12b), one obtains a system of four linear equations in the $k$-$y$ space which can be solved for the four coefficients. These coefficients are inserted into the ansatz for $A$, followed by the inverse Fourier transformation

$$A_\nu(x, y) = \frac{1}{2\pi}\int_{-\infty}^{\infty} A_\nu(k, y)e^{jkx}\,dx. \quad (14)$$

Substituting $A_3(x, y)$ into (2) yields the final result for the eddy current distribution within the slab [12]

$$J_e = -j\frac{\omega\sigma\mu_0 I}{\pi}\int_0^{\infty}\frac{e^{-kh-\gamma y}}{k+\gamma}\,\mathrm{sinc}(k\tau)\cos(ky)\,dk. \quad (15)$$

For the numerical evaluation, the real and imaginary parts of the integrand are separated. In Fig. 3, the distribution of the real and the imaginary parts of $J_e$ along the $y$-axis inside the conducting slab are shown for the numerical evaluation of (15) and for the finite element model based on the parameters shown in the figure. Successive mesh refinements of the finite element model result in very close agreement (less than 5% deviation) between the two models.

Additionally, the real part of $J_e$ is analyzed within the entire $x$-$y$ plane at two different excitation frequencies. It can be seen from Fig. 4(a) and (b) that the current is driven toward the surface of the plate as the frequency increases.

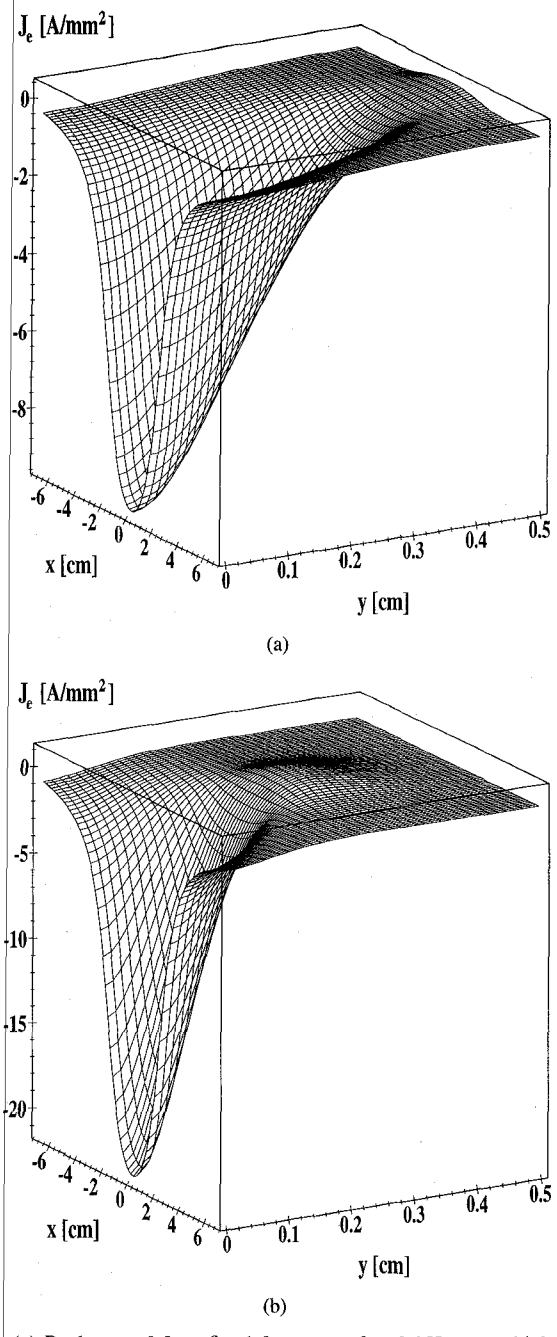


Fig. 4. (a) Real part of $J_e$ at fixed frequency $f = 2$ kHz over thick slab, where $x$ denotes material surface location and $y$ is depth. (b) Real part of $J_e$ at fixed frequency $f = 10$ kHz over thick slab.

### *B. Force Formulation by Using the Moving Image Method*

In order to model the problem more realistically and to obtain a simple approximation for the total force, we assume for the model shown in Fig. 2 now a thin plate with $w \ll h$ and $w \ll \delta$ suspended over a line conductor with $\tau \to 0$ [14].

*1) Theoretical Basis:* Here the magnetic vector potential $\boldsymbol{A}$ consists of two parts: $\boldsymbol{A}_s$ is caused by the source current in the conductor, and $\boldsymbol{A}_e$ is due to the induced eddy currents. This leads, for the electric field $E = J_e/\sigma$, to the form

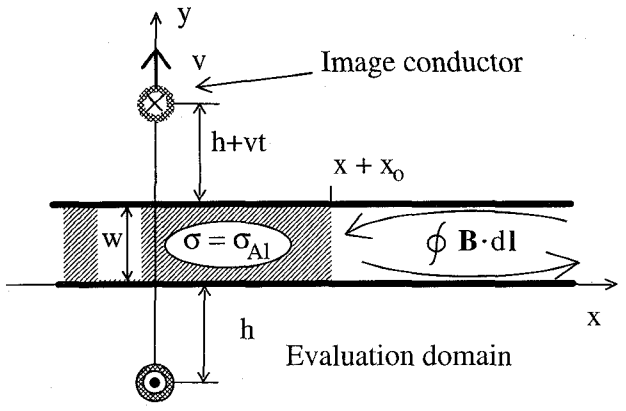


Fig. 5. Path of integration for $\boldsymbol{B}$ field and location of image conductor which recedes with velocity $v$ from starting position $y = h$ ($h \gg w$).

$$\frac{J_e}{\sigma} = -\frac{\partial(A_s + A_e)}{\partial t}. \tag{16}$$

Applying Ampére's law to a cross section of the plate within the $x$-$y$ plane (which extends to the infinitely far edge of the slab as shown in Fig. 5) results under the assumption $w \ll h$ in

$$\frac{1}{\mu_0}\int_{x_0}^{\infty} B_{e,x}\,dx = 2\int_{x_0}^{\infty} wJ_{e,z}\,dx. \tag{17}$$

By differentiating this equation, inserting $J_e$ into (16), and using the relation $B_x = -\partial A/\partial y$, one finds

$$\frac{\partial(A_e + A_s)}{\partial t} = \frac{2}{\mu_0 w\sigma}\frac{\partial A_e}{\partial y} \tag{18}$$

which is valid inside the thin plate [15]. For an assumed step excitation $A_s = A_0\,u(t)$, one can compare (18) to the generic first-order hyperbolic differential equation

$$\frac{\partial \Phi}{\partial t} - v\frac{\partial \Phi}{\partial y} = 0 \tag{19}$$

which has the solution $\phi = \phi(y - vt, t)$, and where the velocity $v$ can be identified as

$$v = \frac{2}{\mu_0 w\sigma}. \tag{20}$$

This means that the flux density and the force on the conductor caused by the eddy currents in the slab can be calculated by replacing the slab with an upward-moving conductor on the upper side of the plate as shown in Fig. 5. This imaginary conductor carries the same current as the original conductor, but with an opposite sign. The $\boldsymbol{B}$ field below the slab caused by the imaginary conductor results in conjunction with the source current $I_0$ in the force per unit length

$$F_y(t) = B_x I_s = u(t)\frac{\mu I_0^2}{2\pi(2h + vt)}. \tag{21}$$

*2) Fourier Transform:* Equation (21) describes the force when excited with a step current $I_s = I_0\,u(t)$. To analyze the step response under a steady-state condition, the Fou-

rier transformation (10) is applied. Since multiplying by $j\omega$ in the frequency domain is equivalent to the Fourier transform of the impulse response, we obtain for the real-part

$$F_y(\omega) = \omega \int_0^\infty \frac{\mu I_0^2}{2\pi(2h + vt)} \sin(\omega t) dt. \tag{22}$$

The imaginary part of $F_y(\omega)$ is irrelevant since only the in-phase component of the $B_x$ field contributes to the resulting force. As a solution to this integral we find

$$F_y(\omega) = \frac{\omega \mu I_s^2}{v\pi} [\pi \cos(\xi) - 2Si(\xi) \cos(\xi) + 2Ci(\xi) \sin(\xi)] \tag{23}$$

where $\xi = \omega h/v$. Here $Si$ denotes the sine integral and $Ci$ denotes the cosine integral as tabulated in [16].

*3) Circuit Approximation:* A simpler analytical expression for $F_y(\omega)$ can be developed by approximating (21) by the sums of two decaying exponential functions

$$F(t) \approx u(t) \frac{\mu_0 I_e^2}{8\pi h} (e^{-t/\tau_1} + e^{-t/\tau_2}) \tag{24}$$

where $\tau_1 = 2h/v$ 1/1.53 and $\tau_2 = 2h/v$ 1/0.228. The error of this approximation is less than 1.26% for $vt/2h \leq 1$. However, for $vt >> 2h$, which is equivalent to extremely small values of $w$ and low frequencies, significant errors occur.

A useful analog for (24) can be established by an equivalent electric circuit which gives the same step response [17]. For instance, the RC circuit in Fig. 6 fits this case. The current $i(t)$ for an excitation with a step voltage is

$$i(t) = V_0 u(t) \frac{1}{R} (e^{-t/RC_1} + e^{-t/RC_2}). \tag{25}$$

Either by inspection or by Fourier transformation of (25), one obtains

$$I(\omega) = V_s \frac{j\omega}{R} \left( \frac{1}{j\omega + \frac{1}{RC_1}} + \frac{1}{j\omega + \frac{1}{RC_2}} \right) \tag{26}$$

for a sinusoidal excitation voltage $V_s = V_0 \cos(\omega t)$.

Expressing the field quantities $\tau_1$, $\tau_2$ and $\mu_0 I^2/8\pi h$ by the equivalent circuit quantities $RC_1$, $RC_2$, and $V_0/R$, we obtain the final result

$$F_y(\omega) = \frac{\mu_0 I^2}{8\pi h} \left( \frac{1}{1 + \left( \frac{1.53}{\omega\sigma\mu_0 wh} \right)^2} + \frac{1}{1 + \left( \frac{0.228}{\omega\sigma\mu_0 wh} \right)^2} \right) \tag{27}$$

for the real part of the force per unit length.

*4) Resulting Force Predictions:* Table I summarizes the forces calculated with the finite element method, the moving image method, and the approximation of (27).

In the finite element model, the 0.1-mm-thick plate consists only of 9 element layers, whereas the 1-mm slab contains 15 rows of elements with a much better aspect ratio. This accounts for the better predictions for the thicker plate. As expected, the approximate solution according to (27) yields more accurate results for higher frequencies or thicker plates.

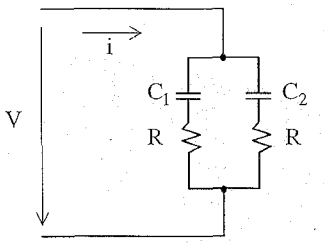


Fig. 6. Circuit analog for moving image model.

TABLE I
RESULTING FORCES PER UNIT LENGTH ON A THIN SLAB FOR $\sigma = 3.7\ 10^7$ $(\Omega m)^{-1}$, $h = 1$ cm AND I = 1 kA

| Thickness w in [mm] | 0.1 | | | 1 | | |
|---|---|---|---|---|---|---|
| Frequency in [kHz] | 1 | 2 | 10 | 1 | 2 | 10 |
| $F_y$ in $[N/m]$ calculated by | | | | | | |
| Finite Element Method | 4.44 | 5.40 | 8.69 | 8.67 | 9.45 | 9.97 |
| Moving Images Method (23) | 3.01 | 4.72 | 8.72 | 8.72 | 9.54 | 9.98 |
| Approximation (26) | 3.28 | 4.98 | 8.89 | 8.89 | 9.67 | 9.99 |

## IV. LEVITATION ARRANGEMENT

### A. Field Predictions

The analytical models prove the accuracy of the finite element approach and point out the basic behavior of the field quantities for two simplified cases. As a next step, a two-dimensional finite element model of an aluminum can above an arrangement of coils is developed. In order to be flexible, this model must be capable of simulating arrangements with one, two, or more coils of various shapes. Furthermore, the horizontal and vertical positions of the can with respect to the coils have to be adjustable.

To meet these requirements and to solve the problem of inhomogeneous mesh densities, which is mainly caused by the very thin mantel of an actual aluminum can, a parametric discretization is developed. To avoid modeling the current displacement within the coils, the associated areas are assigned a high specific resistivity. The aluminum can, which is modeled as a cross-sectional view of the mantel, is represented as a 0.1-mm-thick ring, which consists of four very densely meshed circular segments from where the discretization density decreases with distance. The entire modeling area is surrounded by infinite boundary elements [18].

As an example, a can above an arrangement of two coils (as shown in Fig. 7) is investigated. The computations are performed on a 190 MHz Alpha Station and require for

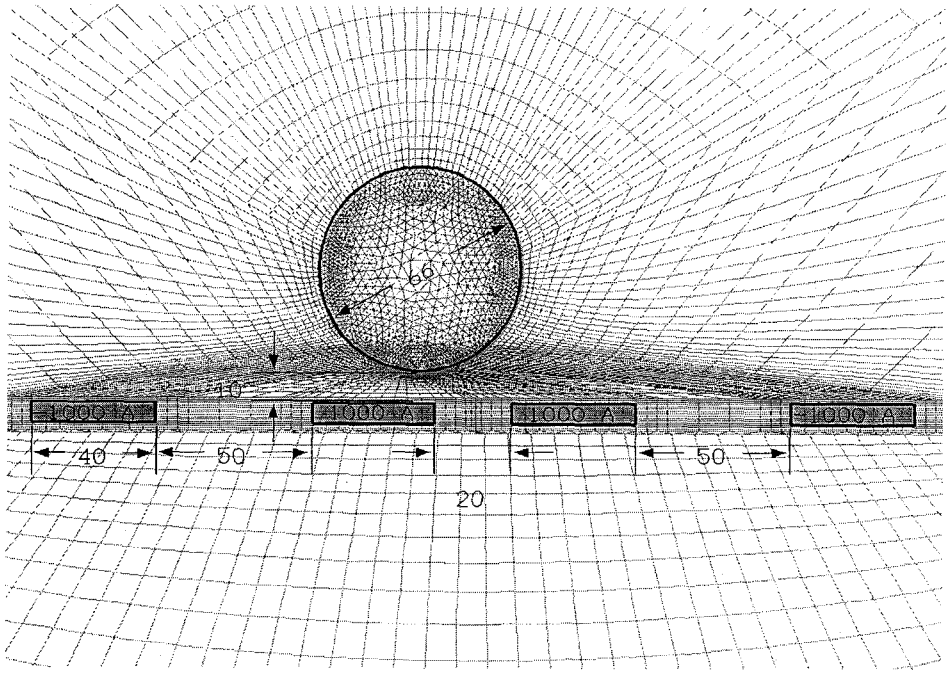


Fig. 7. 2-D mesh in the region of interest with dimensions in (mm) as well as direction and amplitude of source currents.

the mesh generation and finite element solution approximately 40 min CPU time and 95 MByte of disk space.

In Fig. 8(a) and (b), the solution of the finite element simulations is shown. The real part of $A_z$ originates at the coils and is attenuated by the can. For the imaginary part, two distinct extrema on the mantel of the can are observed. Inside the can, the equipotential lines are almost homogeneously distributed, but at the mantel they exhibit a discontinuity.

Although not shown in detail, this finite element model can provide clear insight into the distribution and magnitude of fields, currents, as well as forces. For further verification and demonstration of the permissibility of the underlying assumptions made for this model, measurements on a real eddy current levitation system have to be carried out.

### B. Measurements

For the experiment, an air coil consisting of 170 windings is used (Fig. 9). Its dc resistance and inductance are measured to be $R = 2.30\ \Omega$ and $L = 6.65$ mH. The coil is part of a serial resonance circuit which is driven by a 1000 W transistor amplifier as shown in Fig. 10. The circuit is excited with a sinusoidal signal at the resonance frequency $\omega_{res}$, which can be adjusted by varying the capacity $C$ according to

$$\omega_{res} = \sqrt{\frac{1}{LC} - \frac{R^2}{L^2}}. \tag{28}$$

This arrangement is capable of feeding the coil with a current of up to 10 A over a frequency range from 200 Hz to 20 kHz. The voltage $V_1 = I\sqrt{L/C}$ over the capacitor can attain up to 3 kV.

To determine the exerted force, the weight of the aluminum can is used. The can rests on a 1.6-mm-thick card above the middle of the pancake coil. In order to prevent it from rolling sideways, two stripes of tape on either side of the can serve as small barriers.

At a given frequency, the source current is increased until the upward-directed component of the Lorentz force exceeds the gravity force for the can to be levitated. Since the forces to the left- and right-hand side are equal, no horizontal force will result as long as the can rests on the card above the middle of the coil (see Fig. 11). However, as soon as the can starts to levitate, even a small dislocation to the side results in an immediate sideways acceleration. This unstable equilibrium aids in specifying the "lift-off" time.

*1) Results:* The measured "lift-off" current is taken as an input parameter for the finite element simulation. It is noted that this current has to be multiplied by $170\sqrt{2}$ to take into account the number of windings and the conversion between rms value and amplitude. Since the can material is typically an aluminum alloy, the calculation relies on a conductivity lower than that of pure aluminum [7]. For two frequencies, the results are summarized in Table II.

Comparing the simulated forces to the measurement results provides acceptable agreement. Errors are due to the fact that the simulations are performed in two dimensions which lead to smaller field predictions whereby contributions caused by currents in the $\pm$x-directions are neglected. Furthermore, the heating of the capacitors and

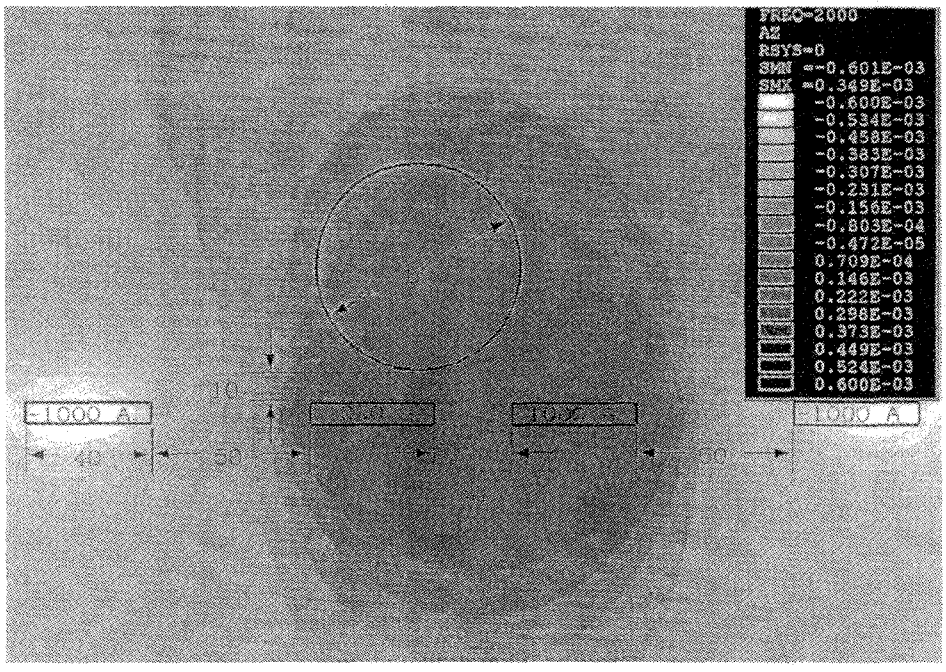


(a)

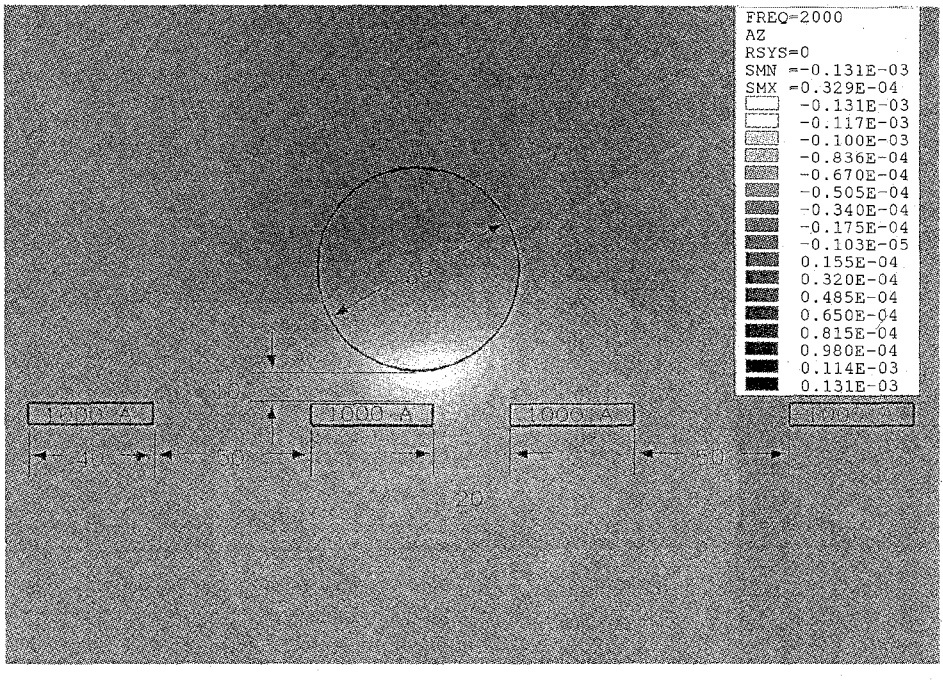


(b)

Fig. 8. (a) Real part of the magnetic vector potential $A$ in [Vs/m] for excitation frequency of 2000 Hz. (b) Imaginary part of the magnetic vector potential $A$ in [Vs/m] for excitation frequency of 2000 Hz.

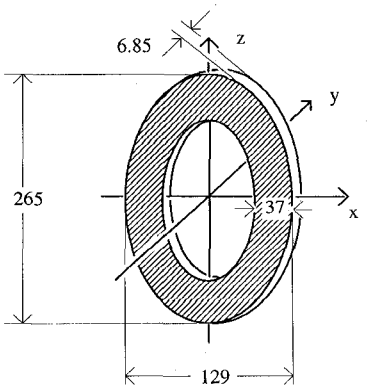


Fig. 9. Pancake coil used in the experiments (dimensions are given in mm).

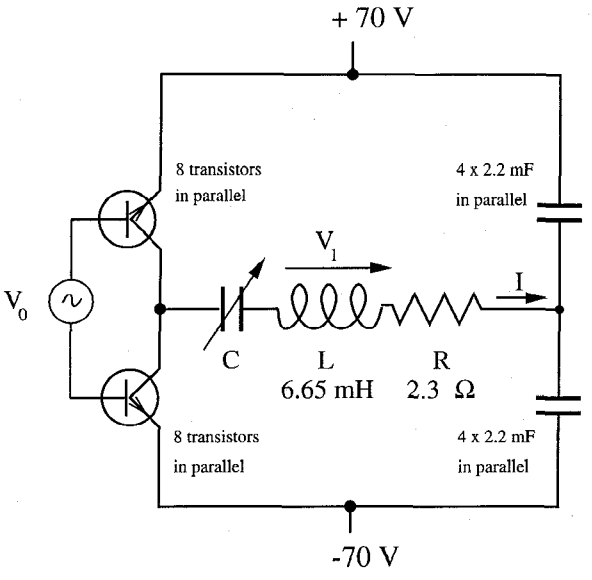


Fig. 10. LRC resonance circuit excited by transistor amplifier.

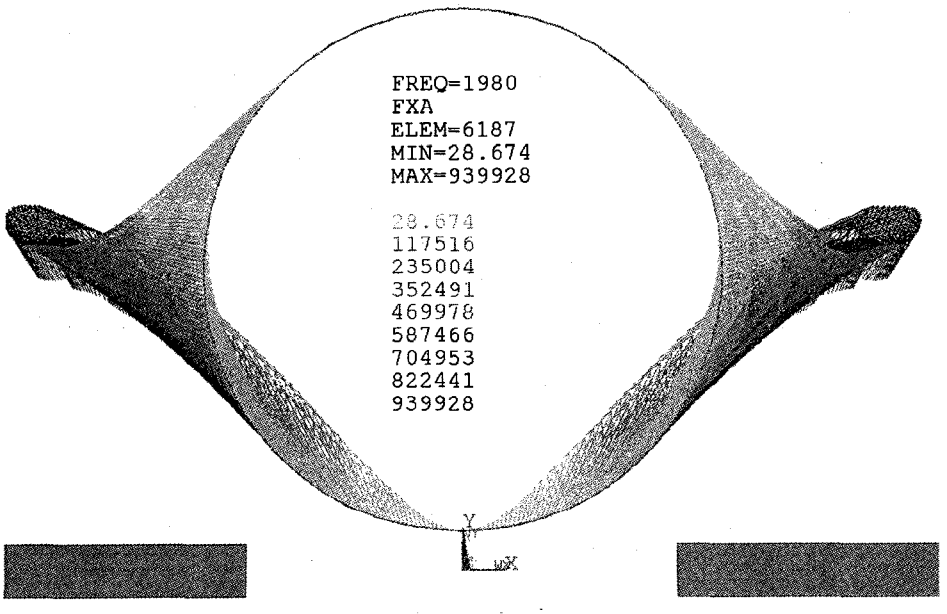


Fig. 11. Can located 1.6 mm above coil. The vectors denote the force density $f$ in [N/m$^2$] for drive current of $I = 6.7$ A at a frequency of 1980 Hz.

TABLE II
MEASURED AND SIMULATED FORCE ON A CAN FOR $\sigma = 1.54\ 10^7\ (\Omega m)^{-1}$, $h = 1.6$ mm

| Frequency [kHz] | 1.980 | 12.25 |
|---|---|---|
| Lift Off Current [A] | 6.2 | 2.7 |
| Gravity Force on Can [N] | 0.17 | |
| Simulated Force [N] | 0.1203 | 0.1596 |

the can causes a drift of the resonance frequency and thus influences the conductivity.

### C. Implementation Considerations

The transistor amplifier arrangement described in Fig. 10 is a relatively inexpensive and adaptable circuit to investigate a wide range of excitation frequencies. However, for industrial applications, much higher forces have to be exerted on the object to be levitated as discussed below.

*1) Currents:* Since the forces are proportional to the square of the current, increasing the current is the most efficient way to achieve higher levitation forces. To generate higher currents, static converters with thyristors could be employed for excitation frequencies up to 10 kHz. These systems, consisting of a thyristor rectifier, a smoothing inductance, and a thyristor converter, are widely used, such as for the inductive melting of metals [19]. Advantages include efficiency of more than 90% and low cost. Furthermore, they can be used for pulsed operation to prevent overheating of the coils.

*2) Drive Frequency:* Another way to enhance the force is to increase the excitation frequency. In Fig. 12 the frequency dependence of the force is compared for two slabs of different thicknesses $w$ according to (27). One finds that for the thicker slab, the force is higher at low frequencies, but reaches saturation earlier than for the thinner slab. The reason for saturation is that at higher frequencies the inductive properties of the material come into effect and add to the reactance in such a way as to increase $J_e$ more slowly. Since at high frequencies the eddy currents are concentrated in a very thin layer beneath the surface, the thickness of the plate has less influence on the force.

For our application, this implies that for the levitation of thinner bodies higher frequencies are desirable. In the mantel of the aluminum cans (0.1 mm), a significant increase in force could be achieved by increasing the frequency up to 10 kHz. Unfortunately, losses in the excitation circuit increase at higher frequencies, requiring a careful optimization for the specific application.

## V. CONCLUSIONS

This paper presents a finite element analysis approach capable of calculating magnetic fields, eddy currents, and forces in flat or circular bodies located above a multiple coil configuration. The validity of the numerical approach is established through comparisons to two analytical methods: the Laplace-transform technique for a conducting half-space, and the moving image method for a thin plate. These methods are important tools in their own right as they can be applied to a range of other problems, for instance, in the area of shielding or magnetic traction.

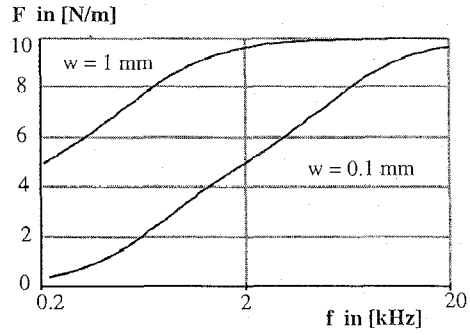


Fig. 12. Force per length unit $F(f)$ exerted within a thin plate of thickness $w$ (logarithmic scale).

The numerically predicted forces are in acceptable agreement with experimental measurements. We intend to employ this numerical method as a flexible tool to design and optimize levitation devices. In particular, future efforts will be directed toward replacing the permanent magnets in the rotating drum shown in Fig. 1 by an array of coils. Furthermore, through variation of drive current and levitation frequency in conjunction with geometric changes of the coils, the separation of small particles such as shredded metal will be analyzed.

## ACKNOWLEDGMENT

Equipment for the experimental part of this project was supplied by Walker Magnetics Group, Inc. The authors express their special appreciation to R. A. Dahlin, Vice-President Engineering, and J. Sedwick for their support and assistance. Furthermore, discussions with Prof. A. Emanuel of the Electrical and Computer Engineering Department at WPI analyzing the thin plate moving image method proved invaluable to this research.

## REFERENCES

[1] H. F. Lund, *The McGraw-Hill Recycling Handbook*. New York: McGraw-Hill, 1993.
[2] A. F. Barton, *Resource Recovery and Recycling*. New York: Wiley, 1979.
[3] A. Iuga, L. Dascalescu, R. Morar, I. Csorvassy, and V. Neamtu, "Corona-electrostatic separators for recovery of waste non-ferrous metals," *J. Electrostatics*, vol. 23, pp. 235–243, 1989.
[4] V. A. Naletova and S. N. Tsurikov, "Redistributing the concentration of the magnetic-fluid disperse phase in a magnetic separator," *Magnetohydrodynamics*, vol. 26, no. 4, pp. 440–445, 1990.
[5] G. H. Nijhof, "Aluminum separation out of household waste using eddy current technique and reuse of metal fraction," *Recourses, Conservation Recycling*, no. 10, pp. 161–169, 1994.
[6] E. Schlömann, "Separation of non-magnetic metals from solid waste by permanent magnets. I. Theory," *J. Appl. Phys.*, vol. 46, no. 11, pp. 5012–5021, 1975.
[7] ——, "Separation of non-magnetic metals from solid waste by permanent magnets. II. Experiments on Circular Discs," *J. Appl. Phys.*, vol. 46, no. 11, pp. 5022–5029, 1975.

[8] D. Fletcher, R. Gerber, P. Lawson, and J. Boehm, "Electromagnetic separation of non-ferrous conductors and non-conductors: Theory and initial experiment," *IEEE Trans. Magn.*, vol. 27, p. 5373, 1991.
[9] D. Fletcher, R. Gerber, L. Tarrant, and T. Reid, "Experimental validation and generalized theory of a single boundary eddy-current separator model," *IEEE Trans. Magn.*, vol. 28, p. 2415, 1992.
[10] D. Fletcher and R. Gerber, "Electromagnetic separation: The prediction and measurement of conductor separability," *IEEE Trans. Magn.*, vol. 29, pp. 3255–3257, Nov. 1993.
[11] M. V. K. Chari and P. P. Sylvester, *Finite Elements in Electrical and Magnetic Field Problems*. New York: Wiley, 1980.
[12] R. Ludwig and X. Dai, "Numerical and analytical modeling of pulsed eddy currents in a conducting half-space," *IEEE Trans. Magn.*, vol. 26, pp. 299–307, Jan. 1990.
[13] R. L. Stoll, *The Analysis of Eddy Currents*. Oxford: Clarendon Press, 1974.
[14] W. M. Saslow, "Maxwell's theory of eddy currents in thin conducting sheets, and applications to electromagnetic shielding and MAGLEV," *Amer. J. Phys.*, vol. 60, no. 8, pp. 693–711, Aug. 1992.
[15] W. R. Smythe, *Static and Dynamic Electricity*. New York: McGraw-Hill, 1950, pp. 403–405.
[16] M. Abramowitz and I. Stegun, *Handbook of Mathematical Functions*. New York: Dover, 1972.
[17] E. J. Tuohy, "Computation of eddy currents, shielding and transient forces in power system equipment by the method of images," *IEEE Trans. Power Apparatus Syst.*, vol. 90, no. 3, pp. 1271–1277, 1971.
[18] I. Kaljevic and S. Saigal, "An infinite boundary element formulation of three-dimensional potential problems," *Int. J. Numer. Methods Eng.*, vol. 35, pp. 2079–2100, 1992.
[19] M. Rudolph and H. Schaefer, *Elektrothermische Verfahren*. Berlin: Springer-Verlag, 1989.

**Martin Woltereck** (SM) was born on Feb. 27, 1971 in Kempten, Germany. He studied electrical power engineering at the Technical University Munich and Worcester Polytechnic Institute. Mr. Woltereck received the Dipl.-Ing. (MSEE) in 1996. He is currently employed at Gesellschaft fuer Anlagen und Reaktorsicherheit. His areas of interest include eddy current modeling, finite elements, and probablistic risk analysis.

**Reinhold Ludwig** (S'83–M'86–SM'90) received the M.S. and Ph.D. degrees in electrical engineering from the University of Wuppertal, Germany, and Colorado State University, Ft. Collins, CO, in 1983 and 1986, respectively.

He has been with the Department of Electrical Engineering, Worcester Polytechnic Institute, Worcester, MA, since 1986 where he is currently a Professor. His research and teaching interests are in the area of electromagnetic and elastodynamic fields as applied to nondestructive material evaluation and medical diagnostics. He held visiting appointments at the University of Kassel, Germany, Hewlett-Packard Company, Andover, MA, and the U.S. Army's Material Technology Laboratory, Watertown, MA.

Dr. Ludwig's current research encompasses pulsed eddy current modeling and the design of special purpose gradient coils for localized MRI imaging.

**William R. Michalson** received the B.S.E.E. degree from Syracuse University in 1981 and the M.S. and Ph.D. degrees from Worcester Polytechnic Institute in 1985 and 1989 respectively.

Since 1981 he has worked full or part-time with the Raytheon Company where he was involved with the development of high performance computer systems for signal and data processing.

In 1985 Dr. Michalson was named an Aldo Miccioli Scholar at Raytheon Company and in 1994 he was named the Joseph Samuel Satin Distinguished Fellow in the Electrical and Computer Engineering Department at WPI. His research interests focus on the computer modeling of physical systems with a main objective being the modeling, test, and evaluation of navigation algorithms for aircraft using the Global Positioning System. He has also been involved with several projects requiring the modeling of electromagnetic phenomena.